Cerebral Cortex, 2022, pp. 1–21

doi: DOI HERE

Using The Virtual Brain to study the relationship between structural and functional connectivity in patients with multiple sclerosis: a multicentre study

Gerard Martí-Juan,[1] Jaume Sastre-Garriga,[2] Eloy Martinez-Heras,[3] Angela Vidal-Jordana,[2] Sara Llufriu,[3] Sergiu Groppa,[4] Gabriel Gonzalez-Escamilla,[4] Maria A. Rocca,[5,6,7] Massimo Filippi,[5,6,7,8,9] Einar A. Høgestøl,[10,11] Hanne F. Harbo,[10,12] Michael A. Foster,[13] Ahmed T. Toosy,[13] Menno M. Schoonheim,[14] Prejaas Tewarie,[15] Giuseppe Pontillo,[13,16,17] Maria Petracca,[18,19] Àlex Rovira,[1,20] Gustavo Deco[21,22] and Deborah Pareto[1,20,*]

[1]Neuroradiology Group, Vall d'Hebron Research Institute (VHIR), Barcelona, Spain, [2]Department of Neurology, Multiple Sclerosis center of Catalonia (Cemcat), Vall d'Hebron University Hospital, Universitat Autònoma de Barcelona (UAB), Barcelona, Spain, [3]Center of Neuroimmunology and Laboratory of Advanced Imaging in Neuroimmunological Diseases (ImaginEM), Hospital Clinic Barcelona, Institut d'Investigacions Biomediques August Pi i Sunyer (IDIBAPS), Universitat de Barcelona, Barcelona, Spain, [4]Department of Neurology, Focus Program Translational Neuroscience (FTN) and Immunotherapy (FZI), University Medical Center of the Johannes Gutenberg University Mainz, Rhine Main Neuroscience Network (rmn2), Mainz, Germany, [5]Neuroimaging Research Unit, Division of Neuroscience, IRCCS San Raffaele Scientific Institute, Milan, Italy, [6]Neurology Unit, IRCCS San Raffaele Scientific Institute, Milan, Italy, [7]Vita-Salute, San Raffaele University, Milan, Italy, [8]Neurorehabilitation Unit, IRCCS San Raffaele Scientific Institute, Milan, Italy, [9]Neurophysiology Service, IRCCS San Raffaele Scientific Institute, Milan, Italy, [10]Department of Neurology, Oslo University Hospital, Oslo, Norway, Department of Psychology, University of Olso, Oslo, Norway, [12]Institute of Clinical Medicine, University of Oslo, Oslo, Norway, [13]Queen Square MS Centre, Dept of Neuroinflammation, Institute of Neurology, University College London, London, United Kingdom, [14]Anatomy and Neurosciences, MS Center Amsterdam, Amsterdam Neuroscience, Amsterdam UMC, Vrije Universiteit Amsterdam, Amsterdam, Netherlands, [15]MS Center Amsterdam, Neurology, Amsterdam Neuroscience, Amsterdam UMC, Vrije Universiteit Amsterdam, Amsterdam, Netherlands, [16]Departments of Advanced Biomedical Sciences and Electrical Engineering and Information Technology, University of Naples "Federico II", Naples, Italy, [17]Department of Radiology and Nuclear Medicine, MS Center Amsterdam, Amsterdam Neuroscience, Amsterdam UMC, Vrije Universiteit Amsterdam, Amsterdam, Netherlands, [18]Department of Neurosciences and Reproductive and Odontostomatological Sciences, University of Naples "Federico II", Naples, Italy, [19]Department of Human Neurosciences, Sapienza University of Rome, Rome, Italy, [20]Radiology (IDI), Vall d'Hebron University Hospital, Barcelona, Spain, [21]Center for Brain and Cognition, Computational Neuroscience Group, Department of Information and Communication Technologies, Universitat Pompeu Fabra, Barcelona, Spain and Institució Catalana de la Recerca i Estudis Avançats, Universitat Pompeu Fabra, Barcelona, Spain
[*]Corresponding author at: Radiology Department, Vall d'Hebron University Hospital, Psg, Vall d'Hebron 119-129, Barcelona 08036, Spain. *E-mail address:* deborah.pareto.idi@gencat.cat (D. Pareto).

Abstract

The relationship between structural connectivity (SC) and functional connectivity (FC) captured from MRI, as well as its interaction with disability and cognitive impairment, is not well understood in people with multiple sclerosis (pwMS). The Virtual Brain (TVB) is an open-source brain simulator for creating personalized brain models using SC and FC. The aim of this study was to explore SC-FC relationship in MS using TVB. Two different model regimes have been studied: stable and oscillatory, with the latter including conduction delays in the brain. The models were applied to 513 pwMS and 208 healthy controls (HC) from 7 different centers. Models were analyzed using structural damage, global diffusion properties, clinical disability, cognitive scores, and graph-derived metrics from both simulated and empirical FC. For the stable model, higher SC-FC coupling was associated with pwMS with low Single Digit Modalities Test (SDMT) score ($F=3.48$, $p<0.05$), suggesting that cognitive impairment in pwMS is associated with a higher SC-FC coupling. Differences in entropy of the simulated FC between HC, high and low SDMT groups ($F=31.57$, $p<1e\text{-}5$), show that the model captures subtle differences not detected in the empirical FC, suggesting the existence of compensatory and maladaptive mechanisms between SC and FC in MS.

Key words: Multiple Sclerosis, The Virtual Brain, Functional Connectivity, Structural Connectivity, MRI

Introduction

Multiple Sclerosis (MS) is a chronic autoimmune disease affecting the central nervous system (Thompson et al., 2018a) and characterized by inflammation, demyelination, and neurodegeneration. MS presents heterogeneously in subjects and causes a wide range of symptoms, including visual impairment, motor disability, and cognitive decline, among others. It has a prevalence of 35,9 per 100,000 in the general population and has been increasing worldwide in the last decade (up by 30% from 2013 to 2020) (Walton et al., 2020). Magnetic resonance imaging (MRI) plays an important role in the diagnosis and in the assessment of the response to treatment (Rovira et al., 2015; Wattjes et al., 2021). Patients with MS (pwMS) present brain and spinal cord atrophy (Sastre-Garriga et al., 2020), focal and diffuse white matter damage (Kutzelnigg et al., 2005), and changes in functional connectivity compared to healthy subjects (HC) (Rocca et al., 2018; D'Ambrosio et al., 2020).

While research on MS has led to important advancements in diagnosis (Thompson et al., 2018b; Rovira and Auger, 2021), therapy and patient care (Tintore et al., 2019), and further understanding of disease mechanisms (Bjornevik et al., 2022), there are many aspects of MS that are still poorly understood. One of the characteristics of MS which is under active research is the link between brain structural damage and functional connectivity (FC) changes (Kutzelnigg et al., 2005). Cognitive or motor function depends on intact communication between brain and spinal chord areas, usually observed through FC. However, the hallmark of MS is structural damage. To understand why individual patients have certain cognitive and and motor/non-motor symptoms it is crucial to understand the relationship between damage to structural connectivity (SC) and FC. Schoonheim et al. (2015) hypothesized that this relationship could be explained by a "compensation mechanism" of the brain: under pressure due to the structural effects of MS, the brain tries to compensate by adapting its FC, but after a certain threshold of damage, it is no longer able to compensate and the condition of the affected person worsens rapidly. Some hypotheses also suggest that this "compensatory" effect can become "maladaptive" (i.e., actually worsen the condition of the patient) (Chard et al., 2021; Schoonheim, 2017), or that both mechanisms may co-exist in early phases of the disease (Groppa et al., 2021). In this context, multimodal models would help to explain functional changes derived from structural damage at the individual patient level.

Recently, there have been efforts in developing whole-brain computational models to model brain functional activity from empirical SC. These models simulate brain activity through a set of differential equations constrained by a given SC and biological assumptions of the brain, creating personalized individual models. A relevant framework for such models is The Virtual Brain (TVB) (Sanz-Leon et al., 2013, 2015), which can generate realistic, synthetic neuronal activity associated with that patient from diffusion and resting state functional MRI.

TVB and other similar frameworks have been used to study brain pathologies such as tumor resection (Aerts et al., 2020), traumatic injuries (Good et al., 2022), epilepsy (Jirsa et al., 2017), and mechanisms of recovery after stroke (Falcon et al., 2016). Depending on the model and parameters, different aspects of brain function can be studied, such as conduction speed using an oscillatory model (Ghosh et al., 2008). Oscillatory models have been shown to generate brain activity close to the resting brain (Petkoski and Jirsa, 2019). TVB has also been proposed to study neurodegenerative diseases. For example, Zimmermann et al. (2018) evaluated how Alzheimer's disease (AD) can affect brain dynamics at the local and global levels, fitting the model individually for each patient and showing that the model parameters were better correlated with cognition and other quantitative MRI measures of the disease than the conventional MRI data. Also on AD, Monteverdi et al. (2022) found subject specific excitation/inhibition profiles across patients at different stages of the disease. Arsiwalla et al. (2015) applied a similar model to

pwMS to study the model's behavior when affected by diffusion lesions, but the disease was not the main focus of the study. Tewarie et al. (2018) used a corticothalamic model to study the relationship between gray matter damage and functional alterations, but their model used estimated values from a population of patients for simulation and did not use specific personalized models.

In this paper, we propose a multicenter analysis of the SC-FC relationship in pwMS and healthy controls (HC) with TVB, using a whole brain computational model to fit the structural and functional patterns of each subject, generating individualized synthetic brain activity and relating it to changes in disability and cognition.

Materials and Methods

Data

Data for this project were provided by the European Magnetic Resonance Imaging in MS (MAGNIMS) consortium. Seven centers have participated in the study, in no specific order: Hospital Clínic, IDIBAPS, Barcelona, Spain; University Medical Center of the Johannes Gutenberg, Mainz, Germany; IRCCS Ospedale San Raffaele, Milan, Italy; Università degli Studi di Napoli "Federico II", Naples, Italy; Oslo University Hospital, Oslo, Norway; Amsterdam Universitair Medische Centra, Amsterdam, Netherlands; UCL Queen Square Institute of Neurology, London, United Kingdom.

Subjects were recruited at each center and data were transferred within a MAGNIMS general framework agreement. For each subject, the centers provided structural T1 and FLAIR MRI, diffusion (DWI) and resting-state functional MRI (rsfMRI), all acquired with 3T scanners. Disability (Expanded Disability Status Scale, EDSS) and cognitive (Symbol Digit Modalities Test, SDMT) outcomes were also provided. PwMS were divided between low / high EDSS (cut-off value of 3, as in (Leray et al., 2013)) and low / high SDMT (cut-off value of 40, as described in (Van Schependom et al., 2014) for differentiating cognitive impairment) for later analysis. Information about the specific imaging protocols provided by each center is available in Supplementary Data 1.

After data processing and quality control (see Section 2.2, Data processing), the final cohort contained a total of 697 subjects, divided between 513 pwMS and 208 HC. Table 1 shows the age and sex (and for pwMS, disease duration, EDSS, and SDMT) of the subjects, divided by center. Further information and distribution of values across centers can be found in Supplementary Data 2.

Data processing

All the available data was processed using the same pipeline, adapting it to the differences in sequences across centres when needed, and with a single machine (Intel® Xeon(R) with 24 cores at 3.50Ghz, 128 GB RAM, Nvidia Quadro RTX 5000 GPU). Subjects were processed in parallel when possible, depending on the number of cores available. Code for MRI preprocessing is available at[1].

Figure 1 a) shows a diagram of the data processing pipeline. Specific details of the pipeline are detailed below.

Structural preprocessing

The 3D-T1 was segmented and parcellated in the Desikan-Killiany atlas with FastSurfer (Henschel et al., 2020, 2022). We included 60 cortical and 16 subcortical regions in our analysis. Grey matter (GM), White matter (WM) and cerebrospinal fluid (CSF) were also segmented for later use in diffusion and rsfMRI preprocessing. Brain parenchymal volume (BPF) was also computed.

[1] `https://github.com/GerardMJuan/FC-SC-data-pipeline`

Table 1. Cohort information.

CENTER	AMSTERDAM	CLINIC	LONDON	MAINZ	MILAN	NAPLES	OSLO
N - HC	48	8	19	26	30	53	24
N - MS	173	58	43	50	56	51	58
N - Total	221	66	62	76	86	104	82
Age - HC	48.41±9.3	29.94±10.6	33.19±7.0	27.85±6.4	37.26±9.3	41.30±11.6	35.12±8.7
Age - MS	48.80±11.3	48.81±9.6	34.43±7.9	35.78±11.6	42.18±9.7	42.48±12.9	40.59±7.2
Sex (%F) - HC	58.33%	87.50%	63.16%	50.00%	40.00%	62.26%	62.50%
Sex (%F) - MS	71.68%	72.41%	62.79%	64.00%	55.36%	66.67%	70.69%
EDSS	3.50 (2.5-5.5)	2.50 (1.5-3.9)	1.50 (1.0-2.0)	1.50 (1.0-2.0)	3.75 (1.5-6.1)	4.50 (2.5-6.0)	2.00 (1.5-2.9)
SDMT	51.21±13.3	46.05±13.4	58.84±9.9	53.12±11.3	50.95±14.3	41.29±13.8	51.48±9.5
DD	15.26±8.7	19.54±9.4	0.41±0.5	4.99±6.6	10.81±9.8	13.29±9.0	10.09±5.3

Age (years), EDSS is shown as (median (Q1-Q3)). SDMT is shown in the format mean±SD. Sex is shown as percentage of females over the total.
Abbreviations: DD = Disease Duration (years). EDSS=Expanded Disability Status Scale. SDMT=Symbol Digit Modality Test. HC=Healthy Control. pwMS=people with Multiple Sclerosis.

Lesion segmentation

Hyperintense white-matter lesions in pwMS were segmented using the Lesion Segmentation Toolbox (Schmidt et al., 2012; Pareto et al., 2016). We also computed the lesion volume fraction (LVF) for all pwMS.

Diffusion preprocessing

Diffusion image processing was performed using Mrtrix3 (Tournier et al., 2019). The steps applied to the data were denoising, Gibbs ringing removal (Kellner et al., 2016), distortion correction (Smith et al., 2004) (including eddy current-induced distortion correction, motion correction, and, if possible, fieldmap-based unwarping using PRELUDE (Jenkinson, 2003) or inhomogeneity distortion correction using TOPUP (Andersson and Sotiropoulos, 2016), and bias correction. Normal appearing white matter (NAWM) mask (obtained from T1 segmentation and then subtracting lesion masks coregistered on T1) were adjusted to each DTI space applying the boundary-based registration inverse transformation matrix between undistorted DWI and T1w to compute its radial diffusivity (RD) and fractional anisotropy (FA) values.

Fiber tracking was performed using a single shell / multishell (depending on center characteristics described in Supplementary data 1) constrained spherical deconvolution (CSD) algorithm to estimate fiber orientation distributions (Tournier et al., 2007; Jeurissen et al., 2014), and using the available segmentation of tissues (GM, WM, and CSF) created during the structural preprocessing, as well as white matter lesion segmentation (considered as WM tissue type, as in (Llufriu et al., 2017)), to create a probabilistic tissue mapping. This mapping was used to perform an anatomical constrained tractography (Smith et al., 2012), using the iFOD2 algorithm (Tournier et al., 2010). 6.000.000 fibers were generated connecting the segmented regions.

To reduce the amount of tracts with biologically unrealistic streamlines, an automatic anatomical exclusion criterion was used to remove implausible streamlines (Martínez-Heras et al., 2015). Then, the SIFT2 algorithm (Smith et al., 2015) was applied to filter the tractogram and adjust the number of streamlines between regions to be proportional to the cross-sectional area of the fibers connecting those two regions, allowing to use of the number of streamlines as a quantitative value of connection.

The final SC matrix was computed as the number of connections or streamlines between regions. Finally, normalization was applied so that the SC largest value was 0.2, as in Deco et al. (2017).

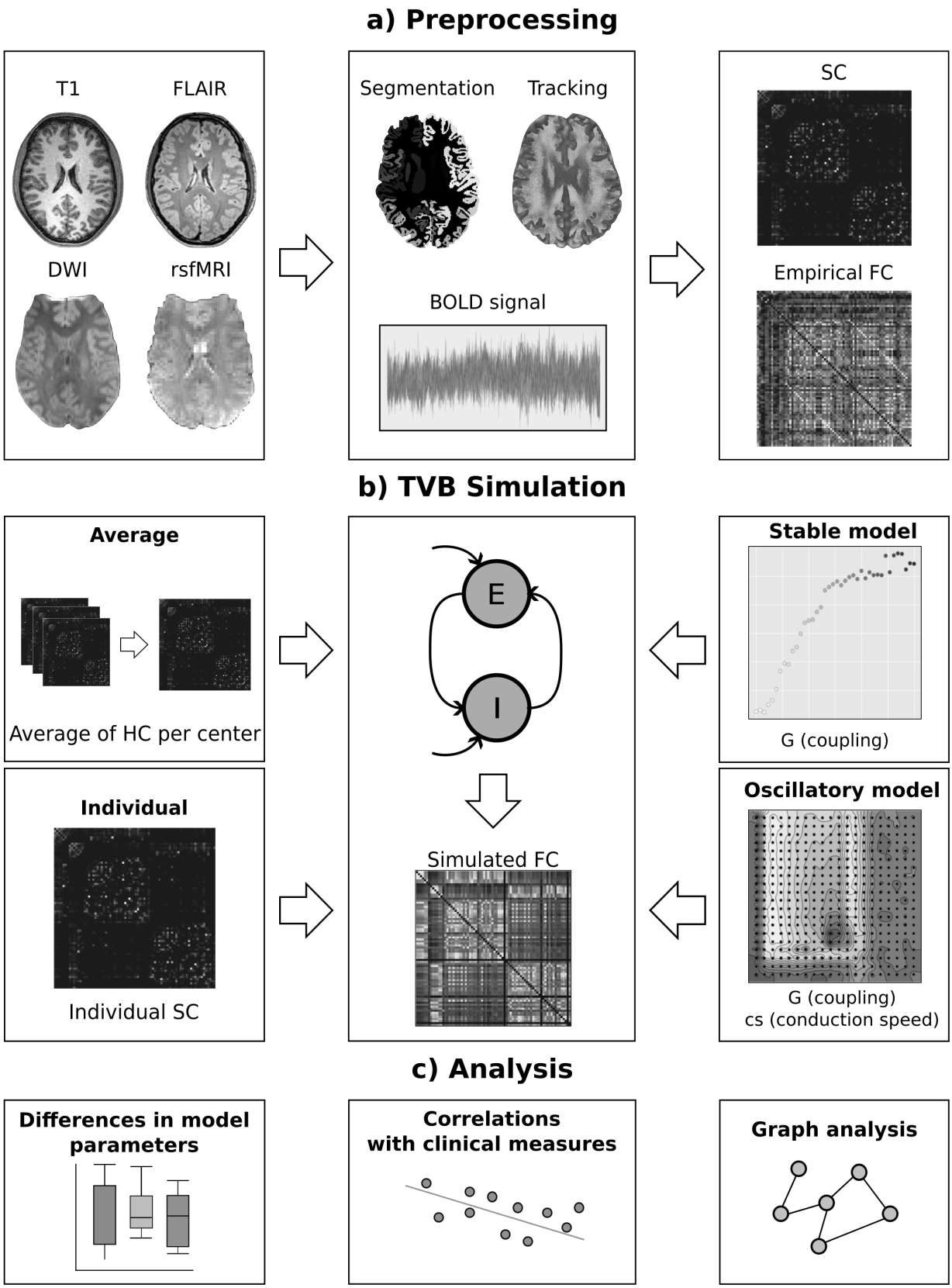

Fig. 1. Diagram of the project pipeline. a) Preprocessing of the data, from MRI sequences to the SC and FC. b) Simulation, with the two experimental procedures (Average, which uses an averaged SC of the healthy controls per center, and individual), and the two model regimes, with the variables to optimize. E=Excitatory, I=Inhibitory. c) Analysis over the fitted model parameters compared to clinical measures and quantitative MRI parameters, and graph analysis of the FC and simFC.

Functional preprocessing

All resting-state functional MRI was processed using the CONN toolbox (Whitfield-Gabrieli and Nieto-Castanon, 2012). The preprocessing steps were: 5 first scans removal, realignment, unwarping, slice timing correction, outlier detection and removal, co-register to structural space, WM/CSF signal regression, low pass filtering (0.001-0.08 Hz), and segmentation. The final FC matrix was defined for each pair of the included regions as the Pearson correlation coefficient between the mean signal from those two regions.

Quality control

Quality control was performed by visually checking the segmentation of the cortical and subcortical regions, the lesion segmentation, and correct registration of structural, diffusion and functional scans. Any subjects that showed poor registration across sequences, bad quality scans, or incorrect segmentations were removed. This was facilitated by an automated script, included in the available code.

Computational model

A dynamic reduced mean field model (DRMF) proposed by (Deco et al., 2014) was chosen as model, due to its use in the study of other neurological diseases, such as AD (Zimmermann et al., 2018). This model is a two-population adaptation of the reduced mean field model proposed by Wong and Wang (2006) that simulates local activity through local and globally connected populations of inhibitory and excitatory groups of neurons. The complete derivation of the reduced model and the justification of its approximations can be found in Deco et al. (2014).

The DRMF model is defined by two coupled excitatory and inhibitory populations for each region or node i, represented by a set of differential equations. Figure 2 a) shows a diagram of the connection between the two populations for a single node. Equations 7 to 2 show the differential equations that define the two populations that characterize the model.

$$\frac{dS_i^{(E)}(t)}{dt} = -\frac{S_i^E}{\tau_E} + (1 - S_i^E)\gamma_E r_i^{(E)} + \sigma \upsilon_i(t) \tag{1}$$

$$\frac{dS_i^{(I)}(t)}{dt} = -\frac{S_i^{(I)}}{\tau_I} + \gamma_I r_i^{(I)} + \sigma \upsilon_i(t), \tag{2}$$

$$r_i^{(E)} = \frac{a_E I_i^{(E)} - b_E}{1 - \exp(-d_E(a_E I_i^{(E)} - b_E))} \tag{3}$$

$$r_i^{(I)} = \frac{a_I I_i^{(I)} - b_I}{1 - \exp(-d_I(a_I I_i^{(I)} - b_I))} \tag{4}$$

$$I_i^{(E)} = W_E I_0 + w_+ J_{NMDA} S_i^{(E)} - J_i S_i^{(I)} + C_i \tag{5}$$

$$I_i^{(I)} = W_I I_0 + J_{NMDA} S_i^{(E)} - S_i^{(I)} \tag{6}$$

$$C_i = G J_{NMDA} \sum_j C_{ij} S_j^{(E)} \tag{7}$$

$S_i^{(E)}$ and $S_i^{(I)}$ (Equations 1, 2) represent the excitatory and inhibitory synaptic gating variable at node i, which modulates based on the firing rate of the corresponding population, with decay regulated by τ_I and τ_E and stochastic white noise ($\upsilon_i(t)$) modulated by an amplitude σ. Population firing rates $r_i^{(E)}$ and $r_i^{(I)}$ (equations 3, 4) are defined by a sigmoidal function on the input currents $I_i^{(I)}$ and $I_i^{(E)}$. These currents (equations 5, 6) are defined by local connections between populations weighted by population-specific parameters, creating a closed loop between the gating variables, currents and firing rates of a single node. Long range connections across nodes are defined by C_i (Equation 7) in the excitatory input current. Those connections are represented in Figure 2, a). $S_i^{(E)}$ and $S_i^{(I)}$ are constrained to be between 0 and 1 due to numerical stability concerns. Equations are solved using Heun's stochastic method.

Two different sets of parameters were used for the DRMF model (Table 2):

- Stable. All parameters have the same values across all nodes except J_i (parameter regulating inhibitory to excitatory coupling), which is fitted iteratively for each node using feedback inhibition control (FIC) (Deco et al., 2014). After adjusting J_i, the simulation is run for the duration of the

rsfMRI acquisition. The model shows stability across its excitatory and inhibitory states, perturbed by connections across nodes and noise (see phase plane, Figure 2, b)).

- Oscillatory. An oscillatory model is able to model signal delays across nodes, introducing another parameter regulating those delays, conduction speed (cs). An exhaustive search was carried out on the excitatory and inhibitory synaptic and recurrent parameters of the original model to obtain, for a single node, the excitatory and inhibitory oscillation frequency was 40Hz, as in Deco et al. (2009). The search space for each fitted parameter is included in Supplementary Data 3. Figure 2, c), shows the dynamics of the model, with a clear oscillatory regime. In addition to the different parameters, a change was introduced in Equation 7, where the time delays are modulated by the new parameter, cs.

$$C_i = GJ_{NMDA} \sum_j C_{ij} S_j^{(E)}(t - \frac{D_{ij}}{cs}), \quad (8)$$

where D_{ij} is the distance between nodes i and j, extracted from the mean tract length across regions for that subject, obtained during fiber tracking analysis.

BOLD activity was generated using the excitatory synaptic activity S_E, through a Balloon-Windkessel hemodynamic model (Friston et al., 2000, 2003), from which a simulated FC (simFC) was generated. The simulated signal has been band passed using the same filter used in the rsfMRI (see Section 2.2.4).

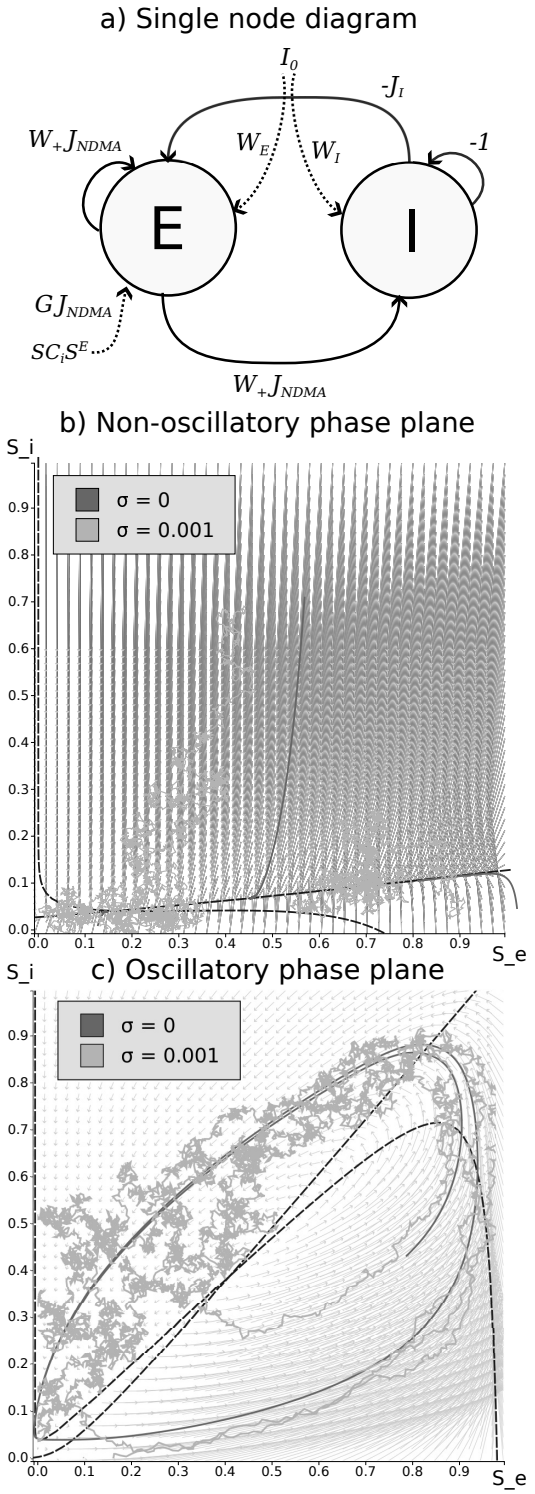

Fig. 2. Diagram and phase plane of the model in both stable and oscillatory regimes for a single node. Each phase plane show trajectories with and without noise. Phase planes are divided using the dotted lines to indicate changes in behavior.

Model optimization

Two different approaches to fit the models were proposed:

- Average HC per center: a connectivity template averaged from the healthy controls was created for each center, and each subject was fitted using the template SC from the corresponding center to their FC. The motivation for this experiment was to observe how the model and its

Table 2. Parameters of the model, for the stable and oscillatory regimes.

Name	Value (stable)	Value (osc.)	Units	Description
a_E	310	310	nC^{-1}	Excitatory synaptic gating constant
b_E	125	125	Hz	Excitatory synaptic gating constant
d_E	0.16	0.16	s	Excitatory synaptic gating constant
τ_E	100	10	ms	Excitatory kinetic parameter, decay time
W_E	1	1.0		Excitatory external input weight
γ_E	$0.641e^{-3}$	$5e^{-3}$	ms	Excitatory kinetic parameter
w_+	1.4	2.4		Local excitatory recurrence parameter
J_{NDMA}	0.15	1.271	nA	Excitatory synaptic coupling parameter
J_I	*	3.099	nA	Local inhibitory synaptic coupling parameter
a_I	615	615	nC^{-1}	Inhibitory synaptic gating constant
b_I	177	177	Hz	Inhibitory synaptic gating constant
d_I	0.087	0.087	s	Inhibitory synaptic gating constant
τ_I	10	20	ms	Inhibitory kinetic parameter, decay time
W_I	0.7	0.45		Inhibitory external input weight
γ_I	$1e^{-3}$	$1e^{-3}$	ms	Inhibitory kinetic parameter
I_0	0.382	0.382	nA	Effective external input
σ	0.001	0.001		Gaussian noise variance

*Obtained iteratively per node.

parameters behave and adapt when trying to adapt to the FC of pwMS without information about the subject's SC. Moreover, this greatly reduces the computational cost of the simulation, as only one simulation per center is needed.

- Individual data: for each subject, their corresponding SC and FC were used to build the model and fit it individually.

Optimization of the model for each subject was carried out by minimizing the difference between real and simulated metastability of the FC and the simFC (Deco et al., 2017). Metastability is defined as the standard deviation of global synchronization of the brain signal at all nodes over time, used to study the coherence of a brain signal. Pearson's uncentered correlation was also calculated between the upper triangular matrix of the FC and the simFC, as very low correlations would suggest a bad optimization.

Model fitting was through a grid search to find the best value of G for the stable model (between 0 and 10), and G (between 0 and 2) and cs (between 0 and 40) for the oscillatory model. Ranges for the parameters were found experimentally, by setting initial ranges from the literature and testing it with a small subset of subjects. We prioritized G and cs as the free parameters of the model for various reasons: They are directly related to the SC, and the other parameters are fixed to obtain the desired model regime (stable and oscillatory). Moreover, adding more free parameters would make the optimization of such a number of subjects computationally infeasible.

For each iteration, the simulation was run 5 times to reduce the influence of noise and results were averaged. A faster implementation of the model in C was used, written by Schirner et al. (2018) and available in[2]. Simulation was done on a High Perfomance Computing (HPC) environment. Code used to run the model is available in[3].

Graph derived metrics

Analyzing FC using graph theory has been proposed as a way to study MS (Fleischer et al., 2019) and to further analyze brain computational models (Deco et al., 2015; Adhikari et al., 2017). Three graph-derived metrics were extracted from both FC and simFC for further analysis, computed independently from the TVB simulation using the *networkx* Python package (code available in the repository):

[2] `https://github.com/BrainModes/fast_tvb`
[3] `https://github.com/GerardMJuan/tvb-wongwang-ms`

- **Entropy**: entropy is a theoretical measure of information that quantifies, for a FC, the diversity of correlations across nodes. Entropy for a FC can be defined as the mean of the entropies of each node.

$$H(i) = -\sum_{j=1}^{N} p_{ij} \log p_{ij}, \tag{9}$$

where p_{ij} is the FC correlation between nodes i and j.

- **Integration**: the integration of a network measures its connectivity between nodes. For N thresholds between 0 and 1 (N=50), the graph is binarized and the size of its largest connected component is measured, normalized by the number of nodes, generating a threshold curve against the threshold value. The integration of the network is the area under the curve.
- **Efficiency**: the efficiency of a network quantifies the small-worldness behavior of the network, that is, that all or most nodes can be reached from another node in few steps. For M pairs of nodes, efficiency is defined as the mean of the inverse of the shortest path length across M. Before calculating the efficiency of the FC, a binarization is needed. The binarization threshold was 0.5, ensuring that only strong connections were considered.

In addition to those three metrics, the mean of the upper triangular matrix of both SC and FC was also calculated, as a simple measure of the connection strength and the correlation, respectively, to discover its relative importance with respect to the fitted parameters.

Experiment design

All the experiments described here were done on the stable and oscillatory regimes, with the average and individual configurations. All statistical analysis was implemented in Python using the statsmodels package.

Differences in G and cs across HC, and pwMS divided in high and low EDSS and SDMT groups were computed using an ANOVA model including three groups (two models, one for EDSS and another one for SDMT), and differences across groups were evaluated with post hoc pairwise Tukey HSD tests. Partial correlations were run between model outcomes (G, cs, best metastability and correlation between sim FC and FC), image derived quantitative MRI parameters (BPF, LVF, FA, RD) and disability and cognitive scores (age, sex and center included as covariates).

Entropy, integration and efficiency of both FC and simFC were compared with G, cs, EDSS and SDMT, via partial correlations (age, sex and center included as covariates). The entropy, integration, and efficiency of FC and simFC were also used to detect differences between HC, high/low EDSS/SDMT for pwMS, using the same ANOVA model procedure described before.

Data availability

Data availability is subject to specific data agreements between Vall d'Hebron Research Institute and each participating MAGNIMS center. Both the MRI and the processed data are available upon request and data transfer approval with the corresponding center.

Results

After applying the data processing pipeline and quality control, a total of 51 subjects were removed for the original cohorts, leaving the total number of subjects at 513 pwMS and 208 HC, as described in Section 2.1. For each model (stable and oscillatory) and configuration (average or individual), the 697 subjects were optimized in parallel, with each subject taking between 3 and 6 hours for the stable model and 12 to 16 hours for the oscillatory model, depending on center.

Figure 3 shows the optimized ΔMetastability for each experiment and model (average and individual, stable and

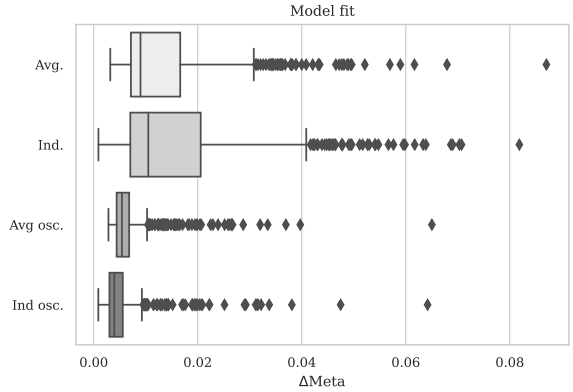

Fig. 3. ΔMetastability for for each experiment, for all subjects.

oscillatory). The oscillatory models achieve a better fit (lower metastability difference between real and simulated FCs) compared to the stable ones. In addition, there were no significant differences in ΔMetastability between average and individual experiments for a given model. The mean correlations between FC and simFC ranged between 0.4 and 0.7 (Supplementary Data 4), being slightly higher for the stable regime.

Figure 4 shows the differences in fitted parameters across HC, and pwMS divided by high/low EDSS and SDMT scores. For the stable model, there were significant differences in the ANOVA when comparing HC, high and low SDMT groups ($F=3.48$, $p<0.05$) with significant pairwise differences between HC and low SDMT, and between high and low SDMT groups, with this last groups having higher values of G. That effect is not observed in the average configuration, nor any other significant effect in the oscillatory model.

Table 3 shows the partial correlations between model parameters and quantitative MS measurements. There were no associations between model parameters (G, c) or model fit values (Corr, ΔMeta) and cognitive, disability and MRI measures of structrual damage in the average experiments (Table 3 a), c)). There were significant (albeit weak, with low r) correlations between G and BPF, FA, and RD, in both stable and oscillatory individual optimizations (Table 3 b), d)).

Table 3. Partial correlations between TVB derived values, and cognitive/disability scores/quantitative MS measurements extracted from the images, corrected by age, sex and center, for each model and configuration.

a) Average stable

	G	Corr	ΔMeta
EDSS	r=0.01	r=0.03	r=-0.03
SDMT	r=0.01	r=-0.00	r=0.04
BPF	r=0.01	r=-0.04	r=-0.02
LVF	r=-0.00	r=0.02	r=0.00
FA	r=-0.01	r=0.00	r=0.02
RD	r=0.00	r=-0.01	r=-0.02

b) Individual stable

	G	Corr	ΔMeta
EDSS	r=0.05	r=0.01	r=-0.01
SDMT	r=-0.02	r=0.05	r=0.04
BPF	r=-0.09*	r=-0.00	r=-0.04
LVF	r=0.03	r=-0.01	r=0.03
FA	r=0.10**	r=-0.03	r=0.01
RD	r=-0.10**	r=0.02	r=-0.02

c) Average oscillatory

	G	cs	Corr	ΔMeta
EDSS	r=-0.01	r=-0.02	r=0.03	r=-0.05
SDMT	r=-0.03	r=0.00	r=0.02	r=0.05
BPF	r=-0.00	r=-0.02	r=-0.02	r=-0.03
LVF	r=0.03	r=-0.01	r=0.01	r=-0.02
FA	r=0.02	r=-0.02	r=-0.01	r=0.01
RD	r=-0.00	r=0.00	r=0.01	r=-0.01

d) Individual oscillatory

	G	cs	Corr	ΔMeta
EDSS	r=0.02	r=-0.03	r=0.03	r=-0.03
SDMT	r=-0.04	r=-0.02	r=0.04	r=0.07
BPF	r=-0.09*	r=0.01	r=0.00	r=-0.00
LVF	r=0.03	r=-0.01	r=0.02	r=-0.01
FA	r=0.11**	r=0.00	r=-0.03	r=0.02
RD	r=-0.10**	r=0.02	r=0.04	r=-0.02

FA: Fractional Anisotropy in normal appearing white matter. RD: Radial Diffusivity in normal appearing white matter. LVF: Lesion Volume Fraction. BPF: Brain Parenchymal fraction. G: Coupling value. Corr: Correlation between simulated and real FC. ΔMeta: Absolute difference in metastabilities between FC and simFC.

*p<0.05.

**p<0.01.

***p<0.001.

Table 4 shows the results of the partial correlations between G and quantitative MS measurements for the EDSS/SDMT subgroups, correcting for age, sex, and center, for individual stable and oscillatory models. G was associated with BPF for higher values of EDSS (being significant for the stable model, -0.23, $p<0.01$), with the same behavior occurring with RD and FA. The association between G and RD/FA in the stable model was significant (0.14, $p<0.01$ and -0.13, $p<0.05$ respectively) in subjects with higher SDMT, while in the oscillatory model that association was present in subjects with lower SDMT (0.23,

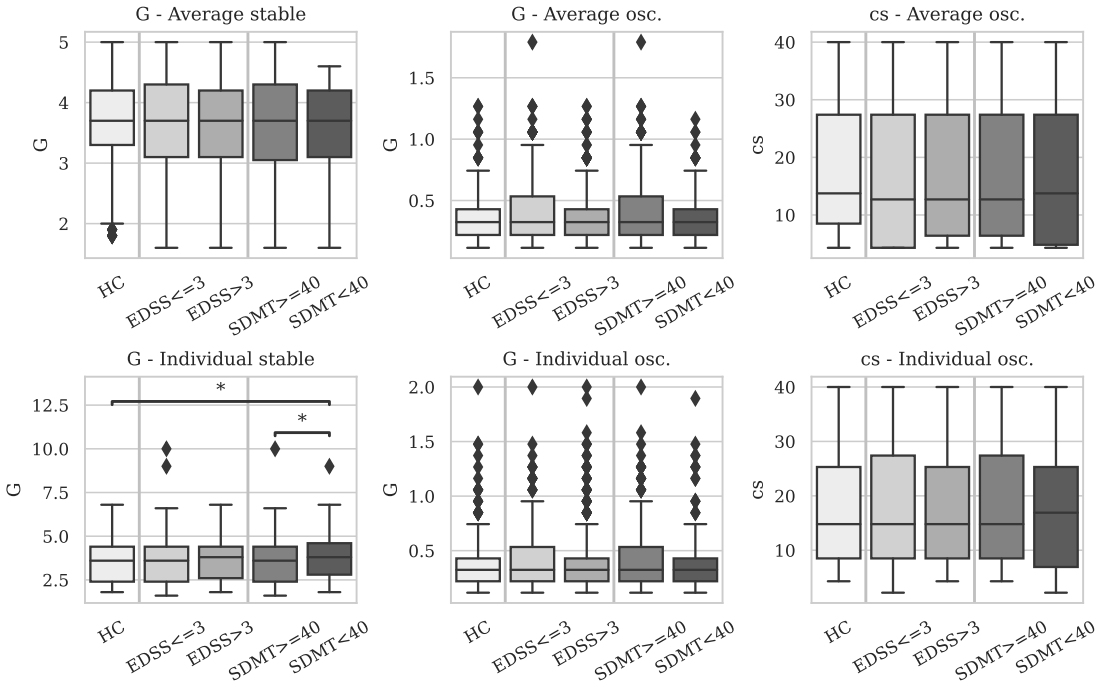

Fig. 4. Comparison of G and cs parameters between HC, and pwMS divided in low/high EDSS and SDMT groups, for each model and configuration.
*: p<0.05.
*p<0.01

Table 4. Partial correlations between G and quantitative MS measurements in groups of patients divided by EDSS and SDMT values, for the individual stable and oscillatory models. Results corrected by age, sex and center.

(a) Individual stable: G

	EDSS<=3	EDSS>3	SDMT>=40	SDMT<40
BPF	r=0.02	r=-0.23**	r=-0.08	r=-0.10
LVF	r=-0.05	r=0.09	r=0.06	r=-0.01
RD	r=0.05	r=0.17*	r=0.14**	r=0.02
FA	r=-0.07	r=-0.14	r=-0.13*	r=-0.02

(b) Individual oscillatory: G

	EDSS<=3	EDSS>3	SDMT>=40	SDMT<40
BPF	r=-0.05	r=-0.15*	r=-0.06	r=-0.18
LVF	r=-0.05	r=0.06	r=-0.06	r=0.10
RD	r=0.01	r=0.22**	r=0.06	r=0.23*
FA	r=0.01	r=-0.24***	r=-0.04	r=-0.28**

LVF: Lesion Volume Fraction. BPF: Brain Parenchymal fraction. FA: Fractional Anisotropy in normal appearing white matter. RD: Radial Diffusivity in normal appearing white matter.

*p<0.05.

**p<0.01.

***p<0.001.

p<0.01 and -0.28, p<0.01, respectively) and high EDSS (0.22, p<0.05 and -0.24, p<0.01, respectively), with comparatively stronger correlations.

Tables 5 and 6 show the partial correlations (corrected by age, sex and center) between graph-derived features from SC, FC and simFC, and G, cs, EDSS and SDMT. SC_{mean} was weakly associated with EDSS and SDMT. G showed a moderate correlation with FC-derived graph features for the average models; for the individual models these correlations disappeared, while the correlation with SC_{mean} was higher (-0.42, p<0.001). When analyzing the relationship of model parameters with graph-derived features from the FC, the stable model showed positive associations with G only for the average configuration: higher values of G were associated with FCs with higher entropy, efficiency and integration. This behavior is not observed in the individual model.

$Entropy_{sim}$ was significantly associated with SDMT and EDSS in all individual configurations, albeit weakly. Strong negative associations between G and simulated features were found ($Entropy_{sim}$ -0.32, $integration_{sim}$ -0.26, $efficiency_{sim}$ -0.42) for the individual stable model. In the individual oscillatory model, higher G was associated with lower

Table 5. Partial correlations (r values) between TVB derived values and graph derived features, stable model. Results corrected by age, sex and center.

	Average stable			Individual stable		
	G	EDSS	SDMT	G	EDSS	SDMT
SC_{mean}	-0.03	-0.10*	0.11**	-0.42***	-0.10*	0.11**
FC_{mean}	0.30***	0.03	0.03	0.06	0.03	0.03
Entropy	0.19***	0.07	0.01	0.04	0.07	0.01
Integration	0.26***	0.06	0.04	0.05	0.06	0.04
Efficiency	0.27***	0.03	0.03	0.06	0.03	0.03
$Entropy_{sim}$	-0.13***	0.01	0.03	-0.32***	-0.10*	0.19***
$Integration_{sim}$	-0.01	0.01	0.04	-0.26***	-0.02	0.06
$Efficiency_{sim}$	-0.45***	0.02	0.03	-0.42***	-0.01	-0.01

SC_{mean}: SC Mean connectivity value. FC_{mean}: FC mean correlation value. Entropy, Integration and Efficiency are computed over the FC, while their simulated counterparts ($_{sim}$) are computed over the simFC.

*p<0.05.

**p<0.01.

***p<0.001.

$entropy_{sim}$ (-0.25) but higher $efficiency_{sim}$ (0.42) and $integration_{sim}$ (0.3), with cs showing opposite associations and no significant relation with $entropy_{sim}$. Similar results were found for the average oscillatory configuration.

Figure 5 shows the differences between entropy, integration and efficiency in simFC across HC and pwMS. $Entropy_{sim}$ showed the largest differences, with differences between HC, low and high SDMT groups in average stable (F=10.41, p<1e-4), individual stable (F=31.5, p<1e-5), and individual oscillatory (F=6.72, p<0.01) models. There were also differences between HC and high/low EDSS in the stable, although the effect was much weaker (F=3.11, p<0.05 for the average stable, F=4.98, p<0.01 for individual), with the tendency being that patients in the group with lower SDMT/higher EDSS have lower values of $Entropy_{sim}$. The same tendency could be seen for efficiency and integration, but no significant differences were observed, apart from a weak difference between HC and low SDMT in $Efficiency_{sim}$ for the average stable model.

Discussion

In this paper, we explored TVB to study the SC-FC relationship in MS. A DRMF-based model with two different configurations was used to create personalized brain simulations through SC-FC coupling and to observe how they relate to disability and cognition in MS. To our knowledge, this is the first study to evaluate personalized whole-brain computational models in MS.

The TVB models achieve a good fit even with incomplete information (HC average), but the oscillatory version is capable of generating a simFC closer to the real one. More specifically, Supplementary data 5 show a qualitative example to better illustrate this point. Differences can be observed between the simFC and the FC: for example, the model struggles to generate homotopic interhemispheric connections that are present in the FC. Supplementary data 6 show a visual example for reference.

Our findings suggest the idea that, for the individual stable configuration, the model needs higher G values compared to HC to fit it to pwMS with a lower SDMT, and to fit pwMS with higher structural and diffusion damage. In other words, structural damage and cognitive impairment appears to make FC more coupled or conditioned by SC through the coupling variable G, as has been observed for MS in other works studying FC (D'Ambrosio et al., 2020). Models with the average configuration do not show this effect. The differences between the average and individual results indicate that including the individual SC is necessary for the model to adapt and capture changes in the brain of the subject (as in (Palesi et al., 2020; Monteverdi et al., 2022)), and it is not able to do so only with the individual FC and a template healthy SC. No differences are observed in the oscillatory model.

The associations found in the stable model can be interpreted as evidence of a compensatory mechanism (Schoonheim et al., 2015; Chard et al., 2021): coupling between SC and FC is not directly related to structural damage, but as the disease progresses and the cognitive impact increases, FC becomes increasingly constrained by the SC. Comparing between average and individual configurations, the model seems

Table 6. Partial correlations (r values) between TVB derived values and graph derived features. Oscillatory model. Results corrected by age, sex and center.

	Average oscillatory				Individual oscillatory			
	G	cs	EDSS	SDMT	G	cs	EDSS	SDMT
SC_{mean}	0.01	0.04	-0.10*	0.11**	-0.18***	0.03	-0.10*	0.11**
FC_{mean}	-0.23***	-0.36***	0.03	0.03	-0.14***	-0.37***	0.03	0.03
Entropy	-0.16***	-0.27***	0.07	0.01	-0.10**	-0.29***	0.07	0.01
Integration	-0.24***	-0.34***	0.06	0.04	-0.14***	-0.36***	0.06	0.04
Efficiency	-0.22***	-0.35***	0.03	0.03	-0.12**	-0.36***	0.03	0.03
$Entropy_{sim}$	-0.33***	0.14***	0.10*	0.02	-0.25***	0.02	-0.09*	0.11**
$Integration_{sim}$	0.40***	-0.37***	0.03	0.03	0.42***	-0.29***	-0.08	0.07
$Efficiency_{sim}$	0.26***	-0.55***	0.03	0.00	0.30***	-0.48***	-0.05	0.00

SC_{mean}: SC Mean connectivity value. FC_{mean}: FC mean correlation value. Entropy, Integration and Efficiency are computed over the FC, while their simulated counterparts ($_{sim}$) are computed over the simFC.

*p<0.05.

**p<0.01.

***p<0.001.

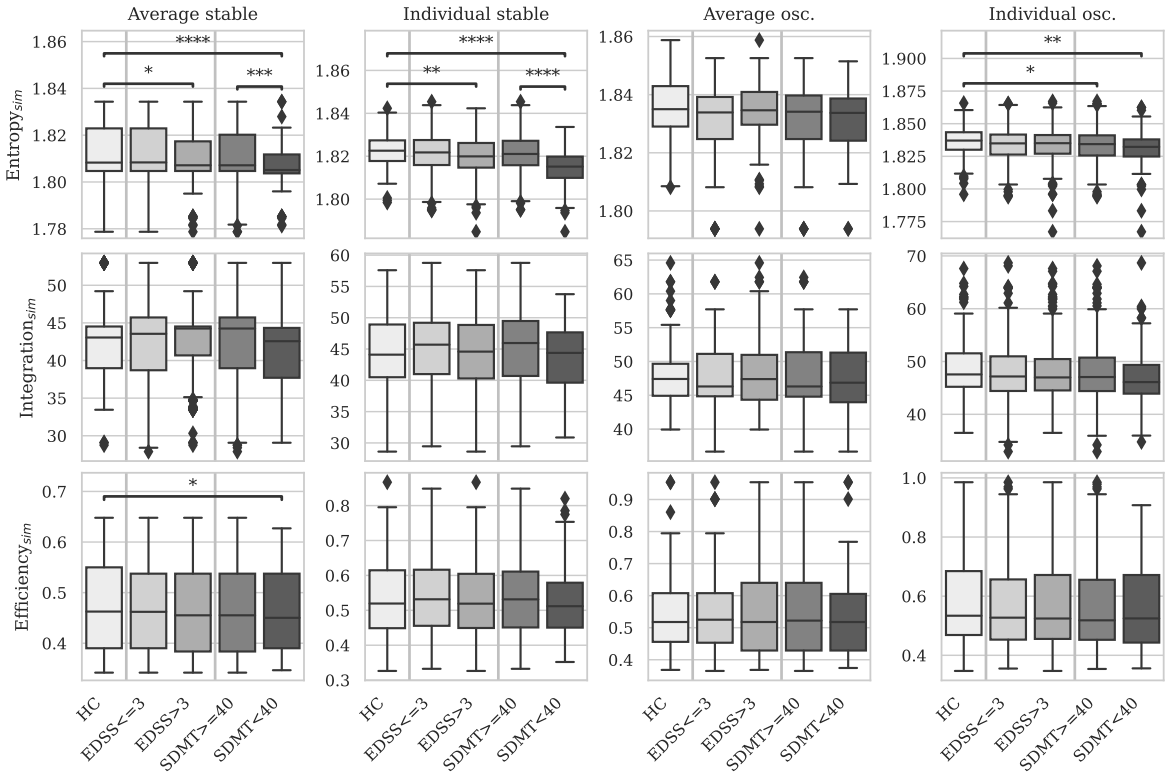

Fig. 5. Comparison of entropy, integration and efficiency of the simulated FC, between HC and pwMS divided in low/high EDSS and SDMT groups, for each model and configuration.
*: p<0.05. **: p<0.01. ***: p<0.001. ****: p<0.0001.

to be more informative when including the individual SC.

The partial correlations found in the patient subgroups of high and low EDSS and SDMT seem to suggest a complex relationship between G, cognition and disability, and show that both models were affected differently by disability and cognition: while the stable model G seemed to correlate better with BPF on pwMS with high EDSS (more disability) and with FA and RD on pwMS with high SDMT (less affected)) the oscillatory G associates only with RD and FA in pwMS with high EDSS/low SDMT (more affected). This could suggest a maladaptive process, where the model tries to adapt both at low cognitive affectation and as the disability increases. However,

these correlations, while significant, are weak.

Differences between the stable and the oscillatory model described in previous paragraphs could be explained by the inclusion of connection delays modulated by cs and tract lengths in the oscillatory model, but no associations betwen cs and EDSS/SDMT/quantitative MS measurements have been found (Supplementary Data 7), so we cannot fully determine it. The optimal cs for each subject found by the oscillatory model does not seem to be related to disability or cognition.

Looking at the relationship of the models with SC_{mean} and FC_{mean}, the main difference between individual and average stable configurations when comparing how G associates with both SC and FC, is that when individual SC information is available, the model relies on it to perform a better simulation. In the oscillatory model the individual configuration accounts for both SC and FC, meaning that the oscillatory model leverage both sources of information to generate a meaningful prediction.

$Entropy_{sim}$ shows weak but significant associations with SDMT and EDSS in individual configurations. The differences found in the stable and oscillatory models between SDMT and EDSS groups suggests that the simulated FC present alterations for subjects with disability or cognitive impairment, so the model is able to incorporate those alterations in its simulation, even if G is not directly associated with EDSS or SDMT. Interestingly, graph-derived measures extracted from the empirical FC show no differences across groups (Supplementary Data 8). SimFC generated by whole-brain computational models being more associated with quantitative neurological measurements than empirical activity is not a new phenomenon. (Zimmermann et al., 2018) found that, for Alzheimer's disease, simFC generated by a Wong-Wang model (equivalent to our individual stable model) was better correlated with decreased cognitive activity than real FC.

Differences between the results using graph-derived features from FC and simFC could be explained by two different reasons. First, the associations with disability and cognitive impairment present in empirical FCs could be obscured by the inherent noise associated with the acquisition of fMRI, whereas simFCs do not have this problem. Another reason could be that the simFC directly reflects the SC changes, while the relationship between real SC and FC is a much more complex process that cannot be completely reflected in the model. This could again support the idea of a compensatory or reorganization mechanism, where pwMS with significant structural damage show low or no disability without cognitive impairment (Schoonheim et al., 2015; Chard et al., 2021). However, to discard any possible biases from the data that could have caused this difference, we would need to replicate the phenomena on a separate cohort of patients.

The low (and, in some cases, lack of) association of the model parameters with disability and cognitive scores does not indicate that the model does not capture relevant disease processes: it just indicates that the fitted parameters to each subject are not directly related to our scale of cognitive impairment and disability. Following the experiments done on the simFC, the model generates an altered FC, with less "healthier" graph-derived measures when the patient presents cognitive effects caused by the disease (See Figure 5).

When taking into account all the results, the stable regime with individual data is the one that shows a better overall performance: it has a reasonable computation time, it is easier to interpret as it has only a free parameter (G), it has a more consistent behavior compared to the oscillatory, and the simulated signal shows slightly more association with disability and cognition. However, the oscillatory regime has certain advantages that should not be overlooked, as it seems to better integrate FC and SC information on the output simFC compared to the stable model. Given the higher computational cost of the oscillatory model and its similarity between the

average and individual configurations, we would recommend using it with a lower number of subjects, or using a SC template when the number of subjects is higher, as this would allow a researcher to explore its dynamics through more detailed ranges of G and cs or longer and more coarse simulations.

This study presents several limitations. Changes in data processing and cortical parcellation have been shown to affect the results obtained by such models (Proix et al., 2016; Aquino et al., 2022), so other atlases with more detailed parcellations could be used. A clear brain region candidate to include would be the cerebellum as it has been strongly linked to MS (Parmar et al., 2018; Tur et al., 2022; Bonacchi et al., 2022) and has been shown to affect TVB simulations (Palesi et al., 2020; Monteverdi et al., 2022). However, due to data and time constraints, it could not be included in this study.

Another limitation of our work concerns our multi-center cohort. We correct for center in our tests, but it has been shown that differences in image acquisitions can significantly alter the tractography and hinder reproducibility across centers. For example, in single shell versus multishell diffusion data, which have been shown to track bias in the tractography reconstruction (Prčkovska et al., 2016; Borrelli et al., 2022). To paliate this, we have used methods that have been shown to reduce variability, such as the CSD algorithm, or the automatic anatomical exclusion criterion used to trim implausible streamlines (Martínez-Heras et al., 2015). However, given the number of different centers we studied, a more complex harmonization method could have been used, such as ComBat (Wachinger et al., 2021).

An initial hypothesis of the oscillatory model was that changes in cs would be associated with demyelination in pwMS (Lubetzki and Stankoff, 2014), but such differences were not found using the proposed model. However, other oscillatory models could be used, such as the Kuramoto or Wilson-Cowan models (Nakagawa et al., 2014; Deco et al., 2009; Petkoski and Jirsa, 2019), using more complex parcellations as mentioned above, or using different connectivity metrics that could better reflect this demyelination (Cercignani et al., 2001).

Furthermore, analyzing changes in dynamic functional connectivity, both real and simulated, could be another interesting option, as it has already been explored before using these models with good results (Cabral et al., 2017). However, this would require longer functional sequences, since sequences acquired in a clinical context, such as those used in this paper, are usually too short. Longitudinal studies would also be useful to further study the compensative/maladaptive hypothesis.

Acknowledgements

We want to thank Michael Schirner and Petra Ritter for their help on setting up the code, and Elisabetta Pagani for her help in solving diffusion data issues during data processing.

Funding

This project was developed as a part of Gerard Martí-Juan ECTRIMS Research Fellowship Program 2021–2022.

Competing interests

G. Martí-Juan has received a MAGNIMS-ECTRIMS fellowship.
J. Sastre-Garriga declares fees from Sanofi, Biogen, Celgene, Merck, Biopass, Novartis, and Roche, and receives research support from Fondo de Investigación en Salud (PI19/00950) from Instituto de Salud Carlos III, Spain.
A. Vidal-Jordana has received support for contracts Juan Rodes (JR16/00024) and receives research support from Fondo de Investigación en Salud (PI17/02162) from Instituto de Salud Carlos III, Spain; and has engaged in consulting and/or participated as speaker in events organized by Novartis, Roche, Biogen, and Sanofi.
S. Llufriu received compensation for consulting services and speaker honoraria from Biogen Idec, Novartis, TEVA,

Genzyme, Sanofi and Merck.

E. Martinez-Heras has nothing to disclose.

S. Groppa has nothing to disclose.

G. Gonzalez-Escamilla has nothing to disclose.

M. A. Rocca received speaker honoraria from Bayer, Biogen, Bristol Myers Squibb, Celgene, Genzyme, Merck Serono, Novartis, Roche, and Teva, and receives research support from the MS Society of Canada and Fondazione Italiana Sclerosi Multipla.

M. Filippi is Editor-in-Chief of the Journal of Neurology and Associate Editor of Human Brain Mapping; received compensation for consulting services and/or speaking activities from Almiral, Alexion, Bayer, Biogen, Celgene, Eli Lilly, Genzyme, Merck-Serono, Novartis, Roche, Sanofi, Takeda, and Teva Pharmaceutical Industries; and receives research support from Biogen Idec, Merck-Serono, Novartis, Roche, Teva Pharmaceutical Industries, Italian Ministry of Health, Fondazione Italiana Sclerosi Multipla, and ARiSLA (Fondazione Italiana di Ricerca per la SLA).

E. A. Høgestøl received honoraria for lecturing and advisory board activity from Biogen, Merck and Sanofi-Genzyme and unrestricted research grant from Merck.

H. F. Harbo has nothing to disclose.

M. A. Foster is supported by an MRC grant (MR/S026088/1).

A. Toosy has been supported by grants from MRC (MR/S026088/1), NIHR BRC (541/CAP/OC/818837) and RoseTrees Trust (A1332 and PGL21/ 10079), has had meeting expenses from Merck, Biomedia and Biogen Idec and was UK PI for two clinical trials sponsored by MEDDAY (MS-ON - NCT02220244 and MS-SPI2 - NCT02220244).

M. M. Schoonheim serves on the editorial board of Neurology and Frontiers in Neurology, receives research support from the Dutch MS Research Foundation, Eurostars-EUREKA, ARSEP, Amsterdam Neuroscience, MAGNIMS and ZonMW and has served as a consultant for or received research support from Atara Biotherapeutics, Biogen, Celgene/Bristol Meyers Squibb, Genzyme, MedDay and Merck.

P. Tewarie has nothing to disclose.

G. Pontillo has received research grants from ECTRIMS-MAGNIMS and ESNR.

M. Petracca discloses travel/meeting expenses from Novartis, Roche and Merck, speaking honoraria from HEALTH&LIFE S.r.l. and honoraria for consulting services from Biogen and research grants from Baroni Foundation.

A. Rovira serves/ed on scientific advisory boards for Novartis, Sanofi-Genzyme, Synthetic MR, TensorMedical, Roche, Biogen, and OLEA Medical, and has received speaker honoraria from Bayer, Sanofi-Genzyme, Merck-Serono, Teva Pharmaceutical Industries Ltd, Novartis, Roche, Bristol-Myers and Biogen, and receives research support from Fondo de Investigación en Salud (PI19/00950) from Instituto de Salud Carlos III, Spain.

G. Deco has nothing to disclose.

D. Pareto has received a research contract from Biogen Idec and receives research support from Fondo de Investigación en Salud (PI18/00823) from Instituto de Salud Carlos III, Spain.

References

Adhikari, M.H., Hacker, C.D., Siegel, J.S., Griffa, A., Hagmann, P., Deco, G., Corbetta, M., 2017. Decreased integration and information capacity in stroke measured by whole brain models of resting state activity. *Brain* 140, 1068–1085. doi:10.1093/brain/awx021.

Aerts, H., Schirner, M., Dhollander, T., Jeurissen, B., Achten, E., Van Roost, D., Ritter, P., Marinazzo, D., 2020. Modeling brain dynamics after tumor resection using The Virtual Brain. *NeuroImage* 213, 116738. doi:10.1016/j.neuroimage.2020.116738.

Andersson, J.L., Sotiropoulos, S.N., 2016. An integrated approach to correction for off-resonance effects and subject movement in diffusion MR imaging. *NeuroImage* 125, 1063–1078. doi:10.1016/j.neuroimage.2015.10.019.

Aquino, K.M., Fulcher, B., Oldham, S., Parkes, L., Gollo, L., Deco, G., Fornito, A., 2022. On the intersection between data quality and dynamical modelling of large-scale fMRI signals.

NeuroImage , 119051doi:10.1016/j.neuroimage.2022.119051.

Arsiwalla, X.D., Zucca, R., Betella, A., Martinez, E., Dalmazzo, D., Omedas, P., Deco, G., Verschure, P.F., 2015. Network dynamics with BrainX3: A large-scale simulation of the human brain network with real-time interaction. *Front. Neuroinformatics* 9, 2. doi:10.3389/fninf.2015.00002.

Bjornevik, K., Cortese, M., Healy, B.C., Kuhle, J., Mina, M.J., Leng, Y., Elledge, S.J., Niebuhr, D.W., Scher, A.I., Munger, K.L., Ascherio, A., 2022. Longitudinal analysis reveals high prevalence of Epstein-Barr virus associated with multiple sclerosis. *Science* 375, 296–301. doi:10.1126/science.abj8222.

Bonacchi, R., Meani, A., Pagani, E., Marchesi, O., Filippi, M., Rocca, M.A., 2022. The role of cerebellar damage in explaining disability and cognition in multiple sclerosis phenotypes: a multiparametric mri study. *J. Neurol.* 269, 3841–3857. doi:10.1007/s00415-022-11021-1.

Borrelli, P., Cavaliere, C., Salvatore, M., Jovicich, J., Aiello, M., 2022. Structural brain network reproducibility: Influence of different diffusion acquisition and tractography reconstruction schemes on graph metrics. *Brain Connect.* 12, 754–767. doi:10.1089/brain.2021.0123. pMID: 34605673.

Cabral, J., Kringelbach, M.L., Deco, G., 2017. Functional connectivity dynamically evolves on multiple time-scales over a static structural connectome: Models and mechanisms. *NeuroImage* 160, 84–96. doi:10.1016/j.neuroimage.2017.03.045.

Cercignani, M., Inglese, M., Pagani, E., Comi, G., Filippi, M., 2001. Mean Diffusivity and Fractional Anisotropy Histograms of Patients with Multiple Sclerosis. *Am J Neuroradiol.* 22, 952–958. doi:10.1002/jmri.21757.

Chard, D.T., Alahmadi, A.A., Audoin, B., Charalambous, T., Enzinger, C., Hulst, H.E., Rocca, M.A., Rovira, À., Sastre-Garriga, J., Schoonheim, M.M., Tijms, B., Tur, C., Gandini Wheeler-Kingshott, C.A., Wink, A.M., Ciccarelli, O., Barkhof, F., Ciccarelli, O., De Stefano, N., Enzinger, C., Filippi, M., Rocca, M.A., Frederiksen, J.L., Gasperini, C., Kappos, L., Palace, J., Rovira, A., Yousry, T., Vrenken, H., 2021. Mind the gap: from neurons to networks to outcomes in multiple sclerosis. *Nat. Rev. Neurol.* 17, 173–184. doi:10.1038/s41582-020-00439-8.

D'Ambrosio, A., Valsasina, P., Gallo, A., De Stefano, N., Pareto, D., Barkhof, F., Ciccarelli, O., Enzinger, C., Tedeschi, G., Stromillo, M.L., Arévalo, M.J., Hulst, H.E., Muhlert, N., Koini, M., Filippi, M., Rocca, M.A., 2020. Reduced dynamics of functional connectivity and cognitive impairment in multiple sclerosis. *Multiple Scler. J.* 26, 476–488. doi:10.1177/1352458519837707.

Deco, G., Jirsa, V., McIntosh, A.R., Sporns, O., Kötter, R., 2009. Key role of coupling, delay, and noise in resting brain fluctuations. *Proc. National Acad. Sci. United States America* 106, 6832–6836. doi:10.1073/pnas.0812500106.

Deco, G., Kringelbach, M.L., Jirsa, V.K., Ritter, P., 2017. The dynamics of resting fluctuations in the brain: Metastability and its dynamical cortical core. *Sci. Reports* 7. doi:10.1038/s41598-017-03073-5.

Deco, G., Ponce-Alvarez, A., Hagmann, P., Romani, G.L., Mantini, D., Corbetta, M., 2014. How local excitation-inhibition ratio impacts the whole brain dynamics. *J. Neurosci.* 34, 7886–7898. doi:10.1523/JNEUROSCI.5068-13.2014.

Deco, G., Tononi, G., Boly, M., Kringelbach, M.L., 2015. Rethinking segregation and integration: Contributions of whole-brain modelling. *Nat. Rev. Neurosci.* 16, 430–439. doi:10.1038/nrn3963.

Falcon, M.I., Riley, J.D., Jirsa, V., McIntosh, A.R., Chen, E.E., Solodkin, A., 2016. Functional mechanisms of recovery after chronic stroke: Modeling with the virtual brain. *eNeuro* 3, 202–208. doi:10.1523/ENEURO.0158-15.2016.

Fleischer, V., Radetz, A., Ciolac, D., Muthuraman, M., Gonzalez-Escamilla, G., Zipp, F., Groppa, S., 2019. Graph Theoretical Framework of Brain Networks in Multiple Sclerosis: A Review of Concepts. *Neuroscience* 403, 35–53. doi:10.1016/j.neuroscience.2017.10.033.

Friston, K.J., Harrison, L., Penny, W., 2003. Dynamic causal modelling. *NeuroImage* 19, 1273–1302. doi:10.1016/S1053-8119(03)00202-7.

Friston, K.J., Mechelli, A., Turner, R., Price, C.J., 2000. Nonlinear responses in fMRI: The balloon model, Volterra kernels, and other hemodynamics. *NeuroImage* 12, 466–477. doi:10.1006/nimg.2000.0630.

Ghosh, A., Rho, Y., McIntosh, A.R., Kötter, R., Jirsa, V.K., 2008. Noise during rest enables the exploration of the brain's dynamic repertoire. *PLoS Comput. Biol.* 4. doi:10.1371/journal.pcbi.1000196.

Good, T., Schirner, M., Shen, K., Ritter, P., Mukherjee, P., Levine, B., McIntosh, A.R., 2022. Personalized Connectome-Based Modeling in Patients with Semi-Acute Phase TBI: Relationship to Acute Neuroimaging and 6 Month Follow-Up. *eNeuro* 9. doi:10.1523/ENEURO.0075-21.2022.

Groppa, S., Gonzalez-Escamilla, G., Eshaghi, A., Meuth, S.G., Ciccarelli, O., 2021. Linking immune-mediated damage to neurodegeneration in multiple sclerosis: could network-based MRI help? *Brain Commun.* 3. doi:10.1093/braincomms/fcab237.

Henschel, L., Conjeti, S., Estrada, S., Diers, K., Fischl, B., Reuter, M., 2020. FastSurfer - A fast and accurate deep learning based neuroimaging pipeline. *NeuroImage* 219, 117012. doi:10.1016/j.neuroimage.2020.117012, arXiv:1910.03866.

Henschel, L., Kügler, D., Reuter, M., 2022. FastSurferVINN: Building resolution-independence into deep learning segmentation methods—A solution for HighRes brain MRI. *NeuroImage* 251, 118933. doi:10.1016/j.neuroimage.2022.118933, arXiv:2112.09654.

Jenkinson, M., 2003. Fast, automated, N-dimensional phase-unwrapping algorithm. *Magn. Reson. Med.* 49, 193–197. doi:10.1002/mrm.10354.

Jeurissen, B., Tournier, J.D., Dhollander, T., Connelly, A., Sijbers, J., 2014. Multi-tissue constrained spherical deconvolution for improved analysis of multi-shell diffusion MRI data. *NeuroImage* 103, 411–426. doi:10.1016/j.neuroimage.2014.07.061.

Jirsa, V.K., Proix, T., Perdikis, D., Woodman, M.M., Wang, H., Bernard, C., Bénar, C., Chauvel, P., Bartolomei, F., Bartolomei, F., Guye, M., Gonzalez-Martinez, J., Chauvel, P., 2017. The Virtual Epileptic Patient: Individualized whole-brain models of epilepsy spread. *NeuroImage* 145, 377–388. doi:10.1016/j.neuroimage.2016.04.049.

Kellner, E., Dhital, B., Kiselev, V.G., Reisert, M., 2016. Gibbs-ringing artifact removal based on local subvoxel-shifts. *Magn. Reson. Med.* 76, 1574–1581. doi:10.1002/mrm.26054, arXiv:1501.07758.

Kutzelnigg, A., Lucchinetti, C.F., Stadelmann, C., Brück, W., Rauschka, H., Bergmann, M., Schmidbauer, M., Parisi, J.E., Lassmann, H., 2005. Cortical demyelination and diffuse white matter injury in multiple sclerosis. *Brain* 128, 2705–2712. doi:10.1093/brain/awh641.

Leray, E., Coustans, M., Le Page, E., Yaouanq, J., Oger, J., Edan, G., 2013. 'Clinically definite benign multiple sclerosis', an unwarranted conceptual hodgepodge: Evidence from a 30-year observational study. *Multiple Scler. J.* 19, 458–465. doi:10.1177/1352458512456613.

Llufriu, S., Martinez-Heras, E., Solana, E., Sola-Valls, N., Sepulveda, M., Blanco, Y., Martinez-Lapiscina, E.H., Andorra, M., Villoslada, P., Prats-Galino, A., Saiz, A., 2017. Structural networks involved in attention and executive functions in multiple sclerosis. *NeuroImage: Clin.* 13, 288–296. doi:10.1016/j.nicl.2016.11.026.

Lubetzki, C., Stankoff, B., 2014. Demyelination in multiple sclerosis, in: Handbook of Clinical Neurology. Elsevier B.V.. volume 122, pp. 89–99. doi:10.1016/B978-0-444-52001-2.00004-2.

Martínez-Heras, E., Varriano, F., Prčkovska, V., Laredo, C., Andorrà, M., Martínez-Lapiscina, E.H., Calvo, A., Lampert, E., Villoslada, P., Saiz, A., Prats-Galino, A., Llufriu, S., 2015. Improved framework for tractography reconstruction of the optic radiation. *PLoS ONE* 10, 1–16. doi:10.1371/journal.pone.0137064.

Monteverdi, A., Palesi, F., Costa, A., Vitali, P., Pichiecchio, A., Ramusino, M.C., Bernini, S., Jirsa, V., Wheeler-Kingshott, C.A.G., D'Angelo, E., 2022. Subject-specific features of excitation/inhibition profiles in neurodegenerative diseases. *Front. Aging Neurosci.* 14. doi:10.3389/fnagi.2022.868342.

Nakagawa, T.T., Woolrich, M., Luckhoo, H., Joensson, M., Mohseni, H., Kringelbach, M.L., Jirsa, V., Deco, G., 2014. How delays matter in an oscillatory whole-brain spiking-neuron network model for MEG alpha-rhythms at rest. *NeuroImage* 87, 383–394. doi:10.1016/j.neuroimage.2013.11.009.

Palesi, F., Lorenzi, R.M., Casellato, C., Ritter, P., Jirsa, V., Wheeler-Kingshott, C.A.G., D'Angelo, E., 2020. The importance of cerebellar connectivity on simulated brain dynamics. *Front. Cell. Neurosci.* 14. doi:10.3389/fncel.2020.00240.

Pareto, D., Sastre-Garriga, J., Aymerich, F.X., Auger, C., Tintoré, M., Montalban, X., Rovira, A., 2016. Lesion filling effect in regional brain volume estimations: a study in multiple sclerosis patients with low lesion load. *Neuroradiology* 58, 467–474. doi:10.1007/s00234-016-1654-5.

Parmar, K., Stadelmann, C., Rocca, M.A., Langdon, D., D'Angelo, E., D'Souza, M., Burggraaff, J., Wegner, C., Sastre-Garriga, J., Barrantes-Freer, A., Dorn, J., Uitdehaag, B.M., Montalban, X., Wuerfel, J., Enzinger, C., Rovira, A., Tintore, M., Filippi, M., Kappos, L., Sprenger, T., 2018. The role of the cerebellum in multiple sclerosis—150 years after Charcot. 89, 85–98. doi:10.1016/j.neubiorev.2018.02.012.

Petkoski, S., Jirsa, V.K., 2019. Transmission time delays organize the brain network synchronization. *Philos. Trans. Royal Soc. A: Math. Phys. Eng. Sci.* 377. doi:10.1098/rsta.2018.0132.

Proix, T., Spiegler, A., Schirner, M., Rothmeier, S., Ritter, P., Jirsa, V.K., 2016. How do parcellation size and short-range connectivity affect dynamics in large-scale brain network models? *NeuroImage* 142, 135–149. doi:10.1016/j.neuroimage.2016.06.016.

Prčkovska, V., Rodrigues, P., Sanchez, A.P., Ramos, M., Andorra, M., Martinez-Heras, E., Falcon, C., Prats-Galino, A., Villoslada, P., 2016. Reproducibility of the structural connectome reconstruction across diffusion methods. *J. Neuroimaging* 26, 46–57. doi:10.1111/jon.12298.

Rocca, M.A., Valsasina, P., Leavitt, V.M., Rodegher, M., Radaelli, M., Riccitelli, G.C., Martinelli, V., Martinelli-Boneschi, F., Falini, A., Comi, G., Filippi, M., 2018. Functional network connectivity abnormalities in multiple sclerosis: Correlations with disability and cognitive impairment. *Multiple Scler. J.* 24, 459–471. doi:10.1177/1352458517699875.

Rovira, À., Auger, C., 2021. Beyond McDonald: updated perspectives on MRI diagnosis of multiple sclerosis. *Expert Review Neurother.* 21, 895–911. doi:10.1080/14737175.2021.1957832.

Rovira, Á., Wattjes, M.P., Tintoré, M., Tur, C., Yousry, T.A., Sormani, M.P., De Stefano, N., Filippi, M., Auger, C., Rocca, M.A., Barkhof, F., Fazekas, F., Kappos, L., Polman, C., Miller, D., Montalban, X., 2015. Evidence-based guidelines: MAGNIMS consensus guidelines on the use of MRI in multiple sclerosis - Clinical implementation in the diagnostic process. *Nat. Rev. Neurol.* 11, 471–482. doi:10.1038/nrneurol.2015.106.

Sanz-Leon, P., Knock, S.A., Spiegler, A., Jirsa, V.K., 2015. Mathematical framework for large-scale brain network modeling in The Virtual Brain. *NeuroImage* 111, 385–430. doi:10.1016/j.neuroimage.2015.01.002.

Sanz-Leon, P., Knock, S.A., Woodman, M.M., Domide, L., Mersmann, J., Mcintosh, A.R., Jirsa, V., 2013. The virtual brain: A simulator of primate brain network dynamics. *Front. Neuroinformatics* 7. doi:10.3389/fninf.2013.00010.

Sastre-Garriga, J., Pareto, D., Battaglini, M., Rocca, M.A., Ciccarelli, O., Enzinger, C., Wuerfel, J., Sormani, M.P., Barkhof, F., Yousry, T.A., De Stefano, N., Tintoré, M., Filippi, M., Gasperini, C., Kappos, L., Río, J., Frederiksen, J., Palace, J., Vrenken, H., Montalban, X., Rovira, À., 2020. MAGNIMS consensus recommendations on the use of brain

and spinal cord atrophy measures in clinical practice. *Nat. Rev. Neurol.* 16, 171–182. doi:10.1038/s41582-020-0314-x.

Schirner, M., Mcintosh, A.R., Jirsa, V., Deco, G., Ritter, P., 2018. Inferring multi-scale neural mechanisms with brain network modelling. *eLIFE* doi:10.7554/eLife.28927.001.

Schmidt, P., Gaser, C., Arsic, M., Buck, D., Förschler, A., Berthele, A., Hoshi, M., Ilg, R., Schmid, V.J., Zimmer, C., Hemmer, B., Mühlau, M., 2012. An automated tool for detection of FLAIR-hyperintense white-matter lesions in Multiple Sclerosis. *NeuroImage* 59, 3774–3783. doi:10.1016/j.neuroimage.2011.11.032.

Schoonheim, M.M., 2017. Functional reorganization is a maladaptive response to injury - Commentary. *Multiple Scler.* 23, 194–196. doi:10.1177/1352458516677593.

Schoonheim, M.M., Meijer, K.A., Geurts, J.J., 2015. Network collapse and cognitive impairment in multiple sclerosis. *Front. Neurol.* 6, 1–5. doi:10.3389/fneur.2015.00082.

Smith, R.E., Tournier, J.D., Calamante, F., Connelly, A., 2012. Anatomically-constrained tractography: Improved diffusion MRI streamlines tractography through effective use of anatomical information. *NeuroImage* 62, 1924–1938. doi:10.1016/j.neuroimage.2012.06.005.

Smith, R.E., Tournier, J.D., Calamante, F., Connelly, A., 2015. SIFT2: Enabling dense quantitative assessment of brain white matter connectivity using streamlines tractography. *NeuroImage* 119, 338–351. doi:10.1016/j.neuroimage.2015.06.092.

Smith, S.M., Jenkinson, M., Woolrich, M.W., Beckmann, C.F., Behrens, T.E., Johansen-Berg, H., Bannister, P.R., De Luca, M., Drobnjak, I., Flitney, D.E., Niazy, R.K., Saunders, J., Vickers, J., Zhang, Y., De Stefano, N., Brady, J.M., Matthews, P.M., 2004. Advances in functional and structural MR image analysis and implementation as FSL. *NeuroImage* 23, 208–219. doi:10.1016/j.neuroimage.2004.07.051.

Tewarie, P., Steenwijk, M.D., Brookes, M.J., Uitdehaag, B.M., Geurts, J.J., Stam, C.J., Schoonheim, M.M., 2018. Explaining the heterogeneity of functional connectivity findings in multiple sclerosis: An empirically informed modeling study. *Hum. Brain Mapp.* 39, 2541–2548. doi:10.1002/hbm.24020.

Thompson, A.J., Banwell, B.L., Barkhof, F., Carroll, W.M., Coetzee, T., Comi, G., Correale, J., Fazekas, F., Filippi, M., Freedman, M.S., Fujihara, K., Galetta, S.L., Hartung, H.P., Kappos, L., Lublin, F.D., Marrie, R.A., Miller, A.E., Miller, D.H., Montalban, X., Mowry, E.M., Sorensen, P.S., Tintoré, M., Traboulsee, A.L., Trojano, M., Uitdehaag, B.M., Vukusic, S., Waubant, E., Weinshenker, B.G., Reingold, S.C., Cohen, J.A., 2018a. Diagnosis of multiple sclerosis: 2017 revisions of the McDonald criteria. *The Lancet Neurol.* 17, 162–173. doi:10.1016/S1474-4422(17)30470-2.

Thompson, A.J., Baranzini, S.E., Geurts, J., Hemmer, B., Ciccarelli, O., 2018b. Multiple sclerosis. *The Lancet* 391, 1622–1636. doi:10.1016/S0140-6736(18)30481-1.

Tintore, M., Vidal-Jordana, A., Sastre-Garriga, J., 2019. Treatment of multiple sclerosis — success from bench to bedside. *Nat. Rev. Neurol.* 15, 53–58. doi:10.1038/s41582-018-0082-z.

Tournier, J.D., Calamante, F., Connelly, A., 2007. Robust determination of the fibre orientation distribution in diffusion MRI: Non-negativity constrained super-resolved spherical deconvolution. *NeuroImage* 35, 1459–1472. doi:10.1016/j.neuroimage.2007.02.016.

Tournier, J.D., Calamante, F., Connelly, A., 2010. Improved probabilistic streamlines tractography by 2 nd order integration over fibre orientation distributions. *Ismrm* 88, 2010.

Tournier, J.D., Smith, R., Raffelt, D., Tabbara, R., Dhollander, T., Pietsch, M., Christiaens, D., Jeurissen, B., Yeh, C.H., Connelly, A., 2019. MRtrix3: A fast, flexible and open software framework for medical image processing and visualisation. *NeuroImage* 202, 116137. doi:10.1016/j.neuroimage.2019.116137.

Tur, C., Grussu, F., Angelis, F.D., Prados, F., Kanber, B., Calvi, A., Eshaghi, A., Charalambous, T., Cortese, R., Chard, D.T., Chataway, J., Thompson, A.J., Ciccarelli, O., Wheeler-Kingshott, C.A.G., 2022. Spatial patterns

of brain lesions assessed through covariance estimations of lesional voxels in multiple sclerosis: The space-ms technique. *NeuroImage: Clin.* 33. doi:10.1016/j.nicl.2021.102904.

Van Schependom, J., D'hooghe, M.B., Cleynhens, K., D'hooge, M., Haelewyck, M.C., De Keyser, J., Nagels, G., 2014. The Symbol Digit Modalities Test as sentinel test for cognitive impairment in multiple sclerosis. *Eur. J. Neurol.* 21, 1–8. doi:10.1111/ene.12463.

Wachinger, C., Rieckmann, A., Pölsterl, S., 2021. Detect and correct bias in multi-site neuroimaging datasets. *Med. Image Anal.* 67, 101879. doi:10.1016/j.media.2020.101879, arXiv:2002.05049.

Walton, C., King, R., Rechtman, L., Kaye, W., Leray, E., Marrie, R.A., Robertson, N., La Rocca, N., Uitdehaag, B., van der Mei, I., Wallin, M., Helme, A., Angood Napier, C., Rijke, N., Baneke, P., 2020. Rising prevalence of multiple sclerosis worldwide: Insights from the Atlas of MS, third edition. *Multiple Scler. J.* 26, 1816–1821. doi:10.1177/1352458520970841.

Wattjes, M.P., Ciccarelli, O., Reich, D.S., Banwell, B., de Stefano, N., Enzinger, C., Fazekas, F., Filippi, M., Frederiksen, J., Gasperini, C., Hacohen, Y., Kappos, L., Li, D.K., Mankad, K., Montalban, X., Newsome, S.D., Oh, J., Palace, J., Rocca, M.A., Sastre-Garriga, J., Tintoré, M., Traboulsee, A., Vrenken, H., Yousry, T., Barkhof, F., Rovira, À., Rocca, M.A., Tintore, M., Rovira, A., 2021. 2021 MAGNIMS–CMSC–NAIMS consensus recommendations on the use of MRI in patients with multiple sclerosis. *The Lancet Neurol.* 20, 653–670. doi:10.1016/S1474-4422(21)00095-8.

Whitfield-Gabrieli, S., Nieto-Castanon, A., 2012. Conn: A Functional Connectivity Toolbox for Correlated and Anticorrelated Brain Networks. *Brain Connect.* 2, 125–141. doi:10.1089/brain.2012.0073.

Wong, K.F., Wang, X.J., 2006. A recurrent network mechanism of time integration in perceptual decisions. *J. Neurosci.* 26, 1314–1328. doi:10.1523/JNEUROSCI.3733-05.2006.

Zimmermann, J., Perry, A., Breakspear, M., Schirner, M., Sachdev, P., Wen, W., Kochan, N.A., Mapstone, M., Ritter, P., McIntosh, A.R., Solodkin, A., 2018. Differentiation of Alzheimer's disease based on local and global parameters in personalized Virtual Brain models. *NeuroImage: Clin.* 19, 240–251. doi:10.1016/j.nicl.2018.04.017.